Structural similarity between the flagellar type III ATPase FliI and F_1-ATPase subunits

Katsumi Imada*†, Tohru Minamino*†, Aiko Tahara*, and Keiichi Namba*†‡

*Graduate School of Frontier Biosciences, Osaka University, 1-3 Yamadaoka, Suita, Osaka 565-0871, Japan; and †Dynamic NanoMachine Project, International Cooperative Research Project, Japan Science and Technology Agency, 1-3 Yamadaoka, Suita, Osaka 565-0871, Japan

Edited by Donald L. D. Caspar, Florida State University, Tallahassee, FL, and approved November 1, 2006 (received for review September 14, 2006)

Construction of the bacterial flagellum in the cell exterior proceeds at its distal end by highly ordered self-assembly of many different component proteins, which are selectively exported through the central channel of the growing flagellum by the flagellar type III export apparatus. FliI is the ATPase of the export apparatus that drives the export process. Here we report the 2.4 Å resolution crystal structure of FliI in the ADP-bound form. FliI consists of three domains, and the whole structure shows extensive similarities to the α and β subunits of F_0F_1-ATPsynthase, a rotary motor that drives the chemical reaction of ATP synthesis. A hexamer model of FliI has been constructed based on the F_1-ATPase structure composed of the $\alpha_3\beta_3\gamma$ subunits. Although the regions that differ in conformation between FliI and the F_1-α/β subunits are all located on the outer surface of the hexamer ring, the main chain structures at the subunit interface and those surrounding the central channel of the ring are well conserved. These results imply an evolutionary relation between the flagellum and F_0F_1-ATPsynthase and a similarity in the mechanism between FliI and F_1-ATPase despite the apparently different functions of these proteins.

bacterial flagellum | crystal structure | F_0F_1-ATPsynthase | type III protein export

The bacterial flagellum is a macromolecular assembly made by ≈30 different proteins with copy numbers ranging from a few to a few tens of thousands (1, 2). The component proteins of the flagellar axial structure are transferred through the central channel of the growing flagellum to its distal end by the flagellar type III export apparatus attached on the cytoplasmic side of the flagellar basal body (3, 4). The flagellar type III protein export apparatus is a complex made of six membrane proteins, FlhA, FlhB, FliO, FliP, FliQ, and FliR, and three soluble proteins, FliH, FliI, and FliJ (5, 6). It is thought that the membrane proteins are located within the putative central pore of the flagellar basal body MS ring to form an export channel, and FliI is attached on the platform made of the cytoplasmic domains of FlhA and FlhB (7). Because the channel diameter through the filament is only 2 nm (8), proteins to be exported must be largely unfolded for entry into and translocation through the channel. *Salmonella* InvC, the FliI homolog of the virulence type III secretion system, has been shown to induce chaperone release from and unfolding of the cognate protein to be secreted in an ATPase-dependent manner (9), suggesting that FliI may act in a similar way.

FliI is a member of the Walker-type ATPase family (10), and it is thought to form a ring-shaped hexamer for protein export (11–14). FliI has significant similarity in its primary sequence to the α and β subunits of F_0F_1-ATPsynthase (14, 15). Although F_1-ATPase requires both the α and β subunits to form the $\alpha_3\beta_3$ hexameric ring to exert its ATPase activity (16), FliI can self-assemble into a hexameric ring in solution, and it shows a cooperative increase in ATPase activity in the presence of ATP and phospholipids (11, 13). Therefore, it is thought that FliI also forms a hexameric ring when it docks to the FlhA–FlhB platform of the flagellar export apparatus (13). FliI oligomerization and its ATP hydrolysis activity are suppressed in cytosol by FliH (17). However, FliH facilitates docking of FliI on to the platform of the export apparatus and recruitment of export substrates to the export apparatus, probably through binding of the $FliH_2FliI$–substrate–chaperone complex to the basal body C ring (7, 18, 19). Thus, FliI displays dynamic interactions with other components in driving flagellar protein export. To understand how FliI oligomerization is regulated and ATP hydrolysis is coupled to the protein export process, we have crystallized and solved the structure of an N-terminally truncated variant of FliI lacking the N-terminal 18 residues, FliI(Δ1–18), in the presence of ADP.

Results

Crystal Structure of FliI(Δ1–18) Monomer. The crystallographic asymmetric unit contains two FliI(Δ1–18) molecules related by a pseudo-2-fold symmetry axis: mol-A, for which the atomic model has been built from Val-25 through Val-456 (missing a linker region from Asn-98 to Gly-107); and mol-B, from Pro-23 through Val-456 (missing a linker region from Asn-98 to Gln-105). The structure can be divided into three domains: the N-terminal domain (Pro-23 to Arg-97), the ATPase domain (Gln-109 to Ile-380), and the C-terminal domain (Thr-381 to Val-456) (Figs. 1 and 2*A*). Both molecules adopt basically the same structure except for the relative orientation of the N-terminal domain to the rest. The N-terminal domain is a compact β barrel structure composed of six β strands. The ATPase domain containing 272 residues shows an α/β fold composed of 10 α helices and 13 β strands. It has the P loop, and the segments from a6 to A2 and from A5 to a9 contain the Walker A and B motif, respectively (Fig. 2*B*) (20). The C-terminal domain consists of three α helices and two loops connecting them. The N-terminal domain is connected to the ATPase domain through a relatively long linker (Asn-98 through Lys-108), most of which is invisible in the electron density map probably because of its conformational flexibility. However, the connectivity is unambiguous because the two residues to be connected are too far apart in the alternative pair, and the present model shows the same arrangement of the two domains as the F_1 subunits. Several N-terminal residues are also missing in the model because of unclear electron densities.

Structural Similarity Between FliI and F_1-ATPase Subunits. A high sequence similarity (29% identity as shown in Fig. 1) has been identified between the ATPase domain of FliI and the F_1-ATPase β subunit, based on which a similar fold has been predicted between

Author contributions: K.I., T.M., and K.N. designed research; K.I., T.M., and A.T. performed research; K.I. analyzed data; and K.I., T.M., and K.N. wrote the paper.

The authors declare no conflict of interest.

This article is a PNAS direct submission.

Abbreviation: PDB, Protein Data Bank.

Data deposition: The atomic coordinates have been deposited in the Protein Data Bank, www.pdb.org (PDB ID code 2DPY).

‡To whom correspondence should be addressed. E-mail: keiichi@fbs.osaka-u.ac.jp.

This article contains supporting information online at www.pnas.org/cgi/content/full/0608090104/DC1.

BIOCHEMISTRY

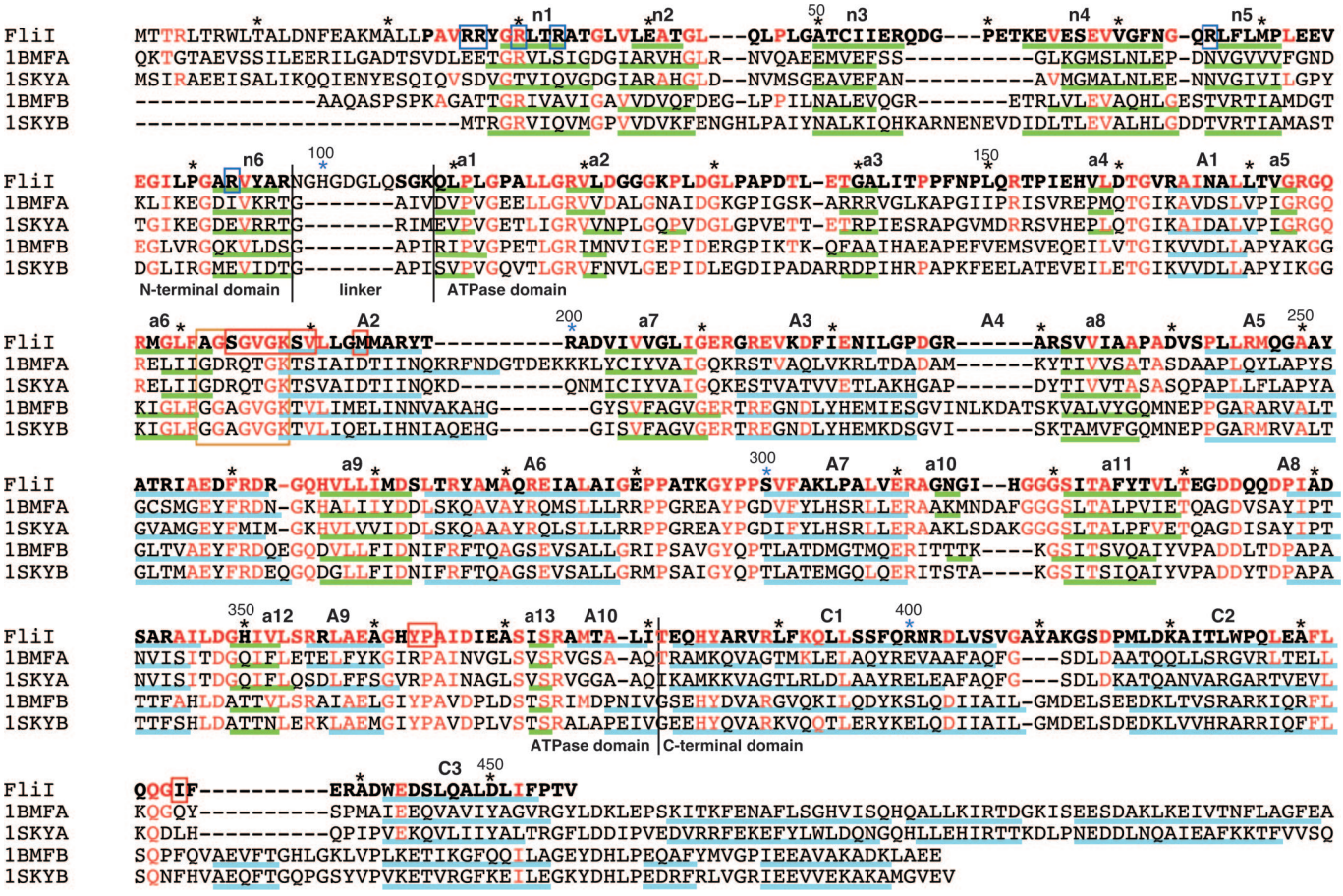

Fig. 1. Structure-based sequence alignment of FliI and the F_1-α/β subunits from bovine mitochondria (1BMFA and 1BMFB) (21) and the thermophilic *Bacillus* PS3 (1SKYA and 1SKYB) (28). The regions of secondary structural elements are shown below each sequence: blue line, α helix; green line, β structure. The secondary structural elements are labeled with initials of three domains (N, A, and C for α helix; n, a, and c for β structure) and numbers. The P loop is shown by the yellow box. The residues conserved between FliI and any of the F_1 subunits are highlighted in red. Red and blue boxes indicate the residues forming a hydrophobic pocket for nucleotide binding and basic residues located on the top surface of the crown-like structure, respectively. The residues included in the molecular model of FliI are shown in bold characters.

them (14). What we have found in the crystal structure of FliI, however, is a surprisingly striking structural similarity to the α and β subunits of F_1-ATPase over the whole molecule (Fig. 2 *C–F*). Direct comparison with the structures of bovine mitochondrial F_1-ATPase α/β subunits [Protein Data Bank (PDB) ID code 1BMF] (21) shows that corresponding C^α atoms (225 of 272 atoms) of the FliI ATPase domain can be superimposed on the three different α subunit structures and three different β subunit structures with root-mean-square (rms) deviations of 1.1~1.3 Å and 1.8~2.1 Å, respectively. Interestingly, the N-terminal and C-terminal domains can also be superimposed onto the α/β subunits with rms deviations of 0.9~1.2 Å and 1.6~2.3 Å, respectively, despite the sequence identities being only 17% and 13%, respectively. These small rms deviations confirm that FliI is structurally very similar to the α/β subunits of F_1-ATPase.

One remarkable difference between them is that the C-terminal domain of FliI is smaller. The first three α helices in the C-terminal domain of FliI are structurally common with those of F_1-ATPase, but the following two or three α helices and the one-turn α helix between the C2 and C3 α helices that are present in the F_1-β subunits are missing in FliI. Because this one-turn α helix contributes to making the hydrophobic pocket for the adenine ring deep, the ATP-binding site of FliI is relatively shallow, just like that of the F_1-α subunit.

The F_1-α/β subunits show different conformations depending on the nucleotide-binding state by changing the relative orientation of the ATPase and C-terminal domains (21). We compared the whole molecule of FliI with that of the F_1-α/β subunits in various states by superimposing corresponding C^α atoms of the ATPase domains (Fig. 2 *C–F*). The conformational difference was measured by rms deviations of C^α atoms of the C1, C2, and C3 α helices. Among the three states of the β subunit in 1BMF [β_{TP}, binding adenosine 5′-[β,γ-imido]triphosphate (AMP-PNP); β_{DP}, binding ADP; β_E, no nucleotide], the β_E structure, which has an open conformation, is most similar to that of FliI with an rms deviation of 3.0 Å (Fig. 2*C*), whereas rms deviations with other conformations are larger than 6.0 Å (Fig. 2 *D* and *E*). The three α subunits show similar rms deviations from 3.5 to 4.2 Å. The most similar conformation among all available ones is found in the ADP-AlF_4 bound structure (PDB ID code 1H8E) (22), which is an inhibited form obtained in the presence of aluminum fluoride and Mg-ADP. The β_{ADP+Pi} subunit in 1H8E, which structurally corresponds to β_E in 1BMF, gives the lowest rms deviation of 2.5 Å (Fig. 2*F*). The β_{ADP+Pi} subunit exhibits a half-closed conformation with Mg-ADP and a sulfate ion that mimics the inorganic phosphate bound (22). This structural similarity is reasonable because our monomeric FliI structure binds ADP, although weakly, as shown later. The bound ADP appears to induce the half-closed conformation.

Nucleotide-Binding Site of FliI. The bound ADP is rather difficult to recognize in the FliI structure probably because of its low occu-

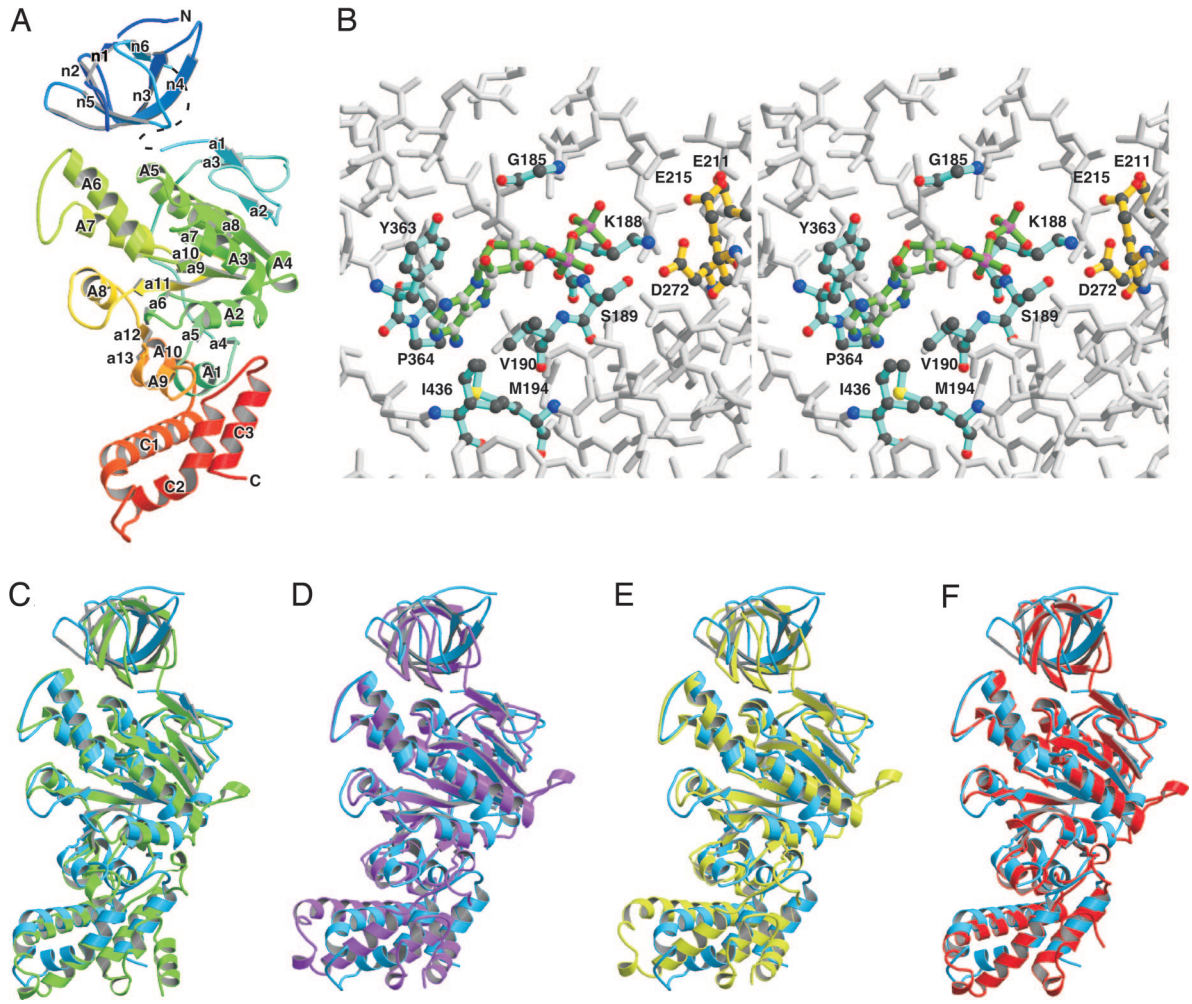

Fig. 2. Structure of FliI(Δ1–18). (*A*) C$^{\alpha}$ ribbon drawing of FliI(Δ1–18). All of the secondary structure elements are labeled as in Fig. 1. The linker connecting the N-terminal and ATPase domains, which is missing in the model, is indicated by a dashed line. (*B*) Close-up stereoview of the nucleotide-binding site. The bound ADP is colored green, and the residues interacting with ADP are shown in cyan. Conserved residues involved in catalysis are indicated by yellow. (*C–F*) Comparison of the relative domain orientation. FliI(Δ1–18) (cyan) is superimposed onto the F_1-β subunits in various states, for which only corresponding atoms in the ATPase domain were used for fitting: (*C*) β_E (green), (*D*) β_{TP} (magenta), (*E*) β_{DP} (yellow) in 1BMF (21), and (*F*) β_{ADP+Pi} (red) in 1H8E (22).

pancy. The density corresponding to the diphosphate is observed on the P loop, and some density corresponding to the adenine ring is seen by the Tyr-363 side chain, although the density of adenosine ribose is poor, and no density is visible for Mg^{2+}. When the β_{ADP+Pi} subunit structure in 1H8E is superimposed onto FliI by using the P loop and the following A3 α-helix, however, the ADP moiety fits nicely in the density [see supporting information (SI) Fig. 4].

Amino acid residues of the F_1-α/β subunits known to be involved in ATP hydrolysis are highly conserved in FliI, some of which are shown around ADP in the nucleotide-binding site (Fig. 2*B*). The di-phosphate binds to the FliI P-loop in the same manner as in the F_1-α/β subunits, which is consistent with previous mutational analysis showing that Lys-188 is required for the ATPase activity (23). Glu-211, Arg-212, Glu-215, Asp-272, and Arg-276, which are expected to be involved with binding Mg^{2+} and the γ-phosphate (21), are relatively far from ADP probably because no sulfate and magnesium ions are bound in the present structure. In agreement with this observation, the corresponding residues of the β_E structure, having the open conformation with no bound nucleotide, are located similarly to those of FliI, even though the present FliI structure is in a half-closed conformation with a low occupancy of ADP. The adenine binds to the hydrophobic pocket formed by Val-190, Met-194, Tyr-363, Pro-364, and Ile-436. The aromatic ring of Tyr-363 is stacked with the adenine ring in a manner similar to that in the β subunit (21). In fact, the Y363S mutation in FliI shows a loss-of-function phenotype (23). These structural similarities strongly suggest that FliI and F_1-ATPase share the similar catalytic pathway for ATP hydrolysis.

The $\alpha_3\beta_3$ hexamer formation is necessary for F_1-ATPase to exert its ATPase activity because Arg-373 in the α subunit stabilizes and increases the negative charge of γ-phosphate in the transition state for catalysis (21, 24, 25). In contrast, FliI still retains the ATPase activity to some extent even in an apparently monomeric state (13). The corresponding arginine Arg-374 of FliI is also conserved among different bacterial species. However, because it is impossible for Arg-374 to play the same role within the same FliI molecule existing as monomer, the mechanism of this base ATPase activity is still unclear. One possible explanation is that the actual monomer is not functional, and transient oligomer formation is responsible. This idea is supported by the fact that FliH keeps FliI monomeric in the cytoplasm by forming the $FliH_2FliI$ complex and thereby inhibits the activity of the ATPase (17).

Hexameric Structure Model of FliI. Because the hexameric ring structure of FliI appears important for flagellar protein export

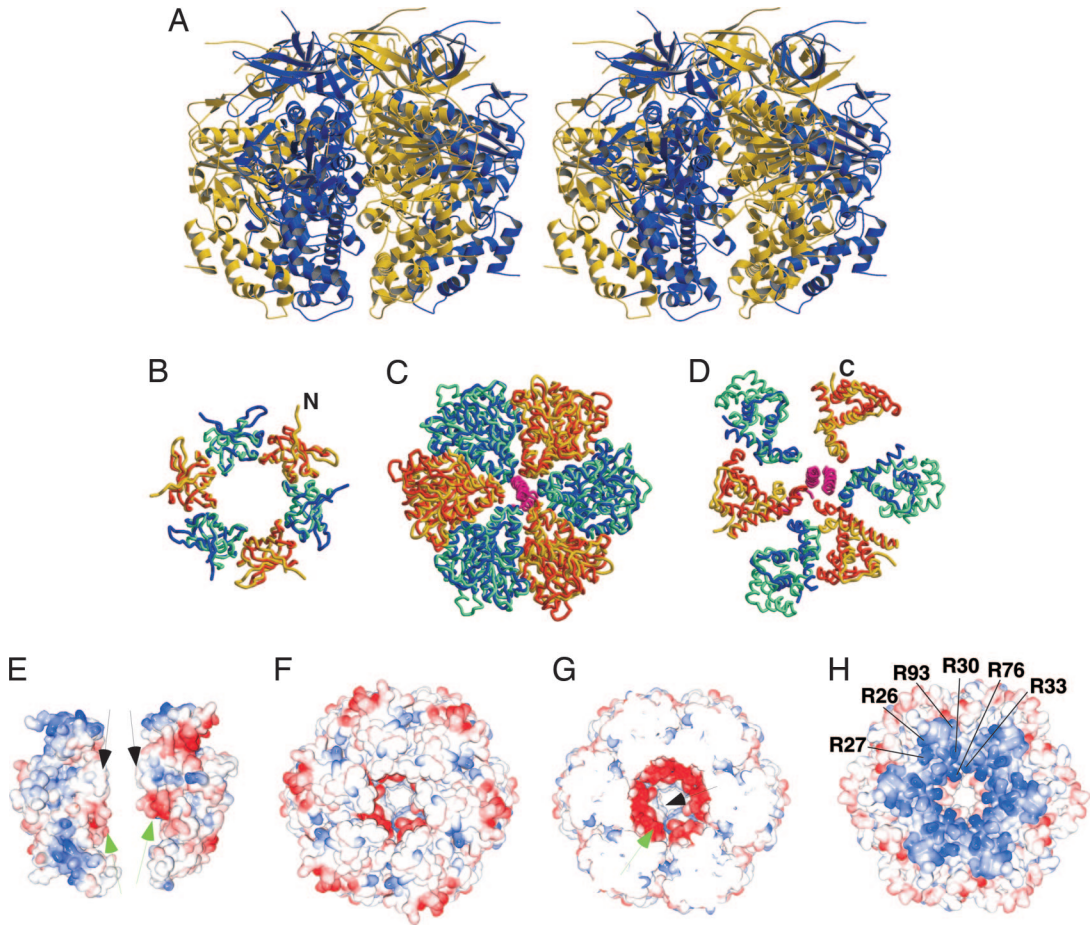

Fig. 3. FliI hexamer model. (*A*) Stereoview of the ribbon diagram. (*B–D*) Superposition of FliI (blue and yellow) onto the α (blue green) and β (orange) subunits of F_1-ATPase [1BMF (ref. 21)]. (*B*) N-terminal domain. (*C*) ATPase domain. (*D*) C-terminal domain. The N and C termini of the model are labeled for one subunit in *B* and *D*, respectively. (*E–H*) Electrostatic surface potential of the FliI hexamer. (*E*) Side view of two opposite subunits. (*F*) End-on view from the C-terminal side. (*G*) End-on view of a cross-section from the C-terminal side. (*H*) End-on view from the N-terminal side. Black and gray arrows indicate the hydrophobic and acidic sleeves, respectively. The surface potential is color coded as blue (positive) or red (negative).

(11, 13), we constructed a hexamer model by using the F_1-ATPase structure of bovine mitochondria (PDB code 1BMF) (21) as a template (Fig. 3 *A–D*). The regions that differ between FliI and the F_1-α/β subunits are all located on the outer surface of the hexamer ring (Fig. 3 *B–D*). The N terminus of the FliI model to which the missing 22 residues are connected also points toward the outside of the hexamer (Fig. 3 *A* and *B*). On the other hand, the main-chain structures constructing the subunit interface and those surrounding the central channel of the ring are well conserved. The loop connecting α helices A6 and A7 forms the hydrophobic sleeve of the central channel (Figs. 2*A* and 3 *E–G*). This structure is highly conserved as well as the unique proline- and glycine-rich sequence (21). Below the hydrophobic sleeve, there is a wider sleeve structure composed of the loop connecting a11 and A8, which is also conserved (Figs. 2*A* and 3 *E–G*). This sleeve is highly acidic in FliI because of three aspartic acids and one glutamic acid located on the loop (Fig. 3*G*).

FliI has structural features of both the α and β subunits of F_1-ATPase. Interestingly, when conserved residues are mapped on the molecular surface of FliI, the residues conserved with the α subunit interact with those conserved with the β subunit at the subunit interface, explaining why FliI can self-assemble into a homohexamer (see SI Fig. 5).

The electrostatic potential mapping on the hexamer demonstrates that the top surface of the crown-like structure formed by the N-terminal domains is positively charged by the contribution of six arginine residues, Arg-26, Arg-27, Arg-30, Arg-33, Arg-76, and Arg-93 (Fig. 3*H*). Because the N-terminal region of FliI is required for the binding to acidic phospholipids and the membrane protein components of the export apparatus (7, 13), these positive charges may mediate such interactions during flagellar protein export.

Discussion

The structural similarity between FliI and F_1-α/β subunits implies a close relation between the bacterial flagellum and F_0F_1-ATPsynthase. FliH has a sequence similarity to both the b and δ subunits of the F_0F_1-ATPsynthase (26). Furthermore, both systems use proton flow through the channel proteins embedded in the cell membrane for mechanical rotation (16, 27), suggesting that these two complex molecular machines have been evolved from a common ancestral system.

The structure of F_1-ATPase is a stable hexameric ring, in which the N-terminal domains of the α/β subunits contribute substantially to the intersubunit interaction by forming 24-stranded β-sheet with the pseudo-6-fold symmetry (21, 28). In contrast, the FliI hexamer is unstable, and the subunit assembly is controlled by external factors. ATP and phospholipids affect the hexamer formation of FliI (11, 13). Oligomerization of FliI is also strongly controlled by a small number of N-terminal residues, and variants of FliI missing those N-terminal residues cannot form the hexamer ring (13, 15), although they still retain

a low-level ATPase activity (13). The N-terminal 18 residues, which are missing in the present structure, include the binding region for FliH, which inhibits the FliI oligomerization but apparently promotes the formation of the active export complex by helping the docking of FliI to the membrane components of the export apparatus (7, 17–19). These observations suggest that the conformation of the short N-terminal stretch is important for the stability of the hexamer. The missing N-terminal region may interact with the extended β-loop-β (n3–n4) region of the neighboring subunit (Fig. 3*B*) and adjust the orientation of the N-terminal domain for stabilizing the hexamer.

AAA ATPases are known to show structural similarities with F_1-ATPase in the core structure of their ATPase domains (29). However, they do not show any similarity in their N-terminal domains; instead, AAA ATPases have their unique domain or subdomain that follows the ATPase domain, contributing to the hexamer formation as well as the ATPase domain (30–32). Thus, the fold and the way the subunits assemble into hexamer are completely different from that of F_1-ATPase and our FliI model.

The extensive structural similarities between the FliI hexamer and F_1-ATPase suggest similar mechanisms. F_1-ATPase is a rotary motor driven by the sequential ATP binding and hydrolysis at the three catalytic sites of the $\alpha_3\beta_3$ ring that couple the changes in the relative orientations of the ATPase and C-terminal domains of the β subunits with the rotation of the γ subunit in the middle of the ring (27, 33, 34). If FliI functions in a similar manner, what would be the equivalent entity to the γ subunit? Specific chaperones involved in the type III secretion system bind to their cognate substrates in the cytoplasm and release them for secretion. InvC, the FliI homolog in the *Salmonella* virulence type III secretion system, has been shown to act as an ATPase-dependent unfoldase that interacts with the chaperone–substrate complexes and unfold the substrates (9). Based on the FliI structure, the potential chaperone-binding site of InvC is mapped on the C-terminal region of the C1 α helix, which corresponds to the region of the β subunit with which the γ subunit interacts. This observation suggests that those chaperones are one of the candidates for the "γ subunit." It may also well be that the FliI hexamer is a linear motor, unfolding and threading export substrates through its central channel by cooperative conformational changes of the subunits, just as speculated for AAA ATPase complexes (35). The structural information on the whole export apparatus will be essential to reveal the export mechanism.

Materials and Methods

Preparation and Crystallization of FliI(Δ1–18). Details of expression, purification, and crystallization of *Salmonella* FliI(Δ1–18) were described in ref. 36. Briefly, monoclinic $P2_1$ crystals of FliI(Δ1–18) with unit cell dimensions $a = 48$ Å, $b = 73$ Å, $c = 126$ Å were grown from a solution containing PEG 8000, calcium acetate, magnesium chloride, and ADP by the hanging-drop vapor diffusion method. Derivatives were prepared by soaking the crystals in a reservoir solution containing K_2PtCl_4 or K_2OsCl_6.

Data Collection and Structure Determination. X-ray diffraction data were collected at synchrotron beamline BL41XU of SPring-8 (Harima, Japan). The statistics of the data were described in ref. 36. The crystals were frozen in liquid nitrogen. Because the derivative crystals were highly sensitive to x-ray, we used a helium cryo-cooling device to reduce the radiation damage. The data were processed with MOSFLM (37) and scaled with SCALA (38). After initial scaling, frames that did not show evidence of significant radiation damage were selected and rescaled. Removal of damaged data were essential for phasing. Phase calculation was performed by using SOLVE (39). The best electron density map was obtained from the MIRAS phase by using the two heavy atom derivatives with anomalous data at the peak wavelengths followed by density modification with DM (38). The model was constructed with O (40). The model was refined at 2.4 Å by using program X-PLOR (41) and, for the final stage, CNS (42). During the refinement process, manual modification was performed by using omit map. The refinement converged to an *R* factor of 24.4% and a free *R* factor of 29.5%. The Ramachandran plot showed that 84.7% and 13.4% residues were located in the most favorable and allowed region, respectively. Structural refinement statistics are summarized in Table 1.

Table 1. X-ray refinement statistics

Measurement	Value
Resolution range, Å	46–2.4 (2.55–2.4)
No. of reflections working	33,945 (5,312)
No. of reflections test	1,680 (262)
R_w, %	24.4 (29.6)
R_{free}, %	29.6 (36.0)
rms deviation bond length, Å	0.007
rms deviation bond angle, °	1.4
B factors	
Protein atoms	49.6
Ligand atoms	130.7
Solvent atoms	50.4
Ramachandran plot, %	
Most favored	84.7
Additionally allowed	13.4
Generously allowed	1.9
Disallowed	0
No. of protein atoms	6,445
No. of ligand atoms*	27
No. of solvent atoms	133

Values in parentheses are for the highest-resolution shell.
$R_w = \Sigma \| F_o \| - \| F_c \| / \Sigma | F_o |$, $R_{free} = \Sigma \| F_o \| - \| F_c \| / \Sigma | F_o |$
*Because of poor electron density, the ADP bound to mol-A was not modeled.

Model Building of the Hexamer. The hexamer model was built based on the F_1-ATPase structure (PDB ID code 1BMF) as a template. The N-terminal domain and the other two domains were fitted separately on the template. We first determined the common structural regions by manually superimposing FliI to the template, and we carried out the least-squares fitting with a program LSQAB in the CCP4 package (38). Because of the conformational variation of the C-terminal domain of F_1-α/β subunits, we used only the common region of the ATPase domain for fitting the ATPase and C-terminal domains.

We thank R. M. Macnab, who suddenly passed away in September 2003, and M. Kihara for invaluable discussion, continuous support, and encouragement; N. Shimizu, M. Kawamoto, K. Hasegawa, and M. Yamamto at SPring-8 for technical help in use of beamlines; and F. Oosawa and S. Asakura for continuous support and encouragement. This work was partially supported by Grants-in-Aid for Scientific Research 16310088 and 18074006 (to K.I.) and 16087207 (to K.N.) and National Project on Protein Structural and Functional Analyses (to K.I.) from the Ministry of Education, Culture, Sports, Science, and Technology of Japan.

1. Berg HC (2003) *Annu Rev Biochem* 72:19–54.
2. Macnab RM (2003) *Annu Rev Microbiol* 57:77–100.
3. Macnab RM (2004) *Biochim Biophys Acta* 1694:207–217.
4. Minamino T, Namba K (2004) *J Mol Microbiol Biotechnol* 7:5–17.
5. Minamino T, Macnab RM (1999) *J Bacteriol* 181:1388–1394.
6. Minamino T, Macnab RM (2000) *Mol Microbiol* 35:1052–1064.
7. Minamino T, González-Pedrajo B, Kihara M, Namba K, Macnab RM (2003) *J Bacteriol* 185:3983–3988.
8. Yonekura K, Maki-Yonekura S, Namba K (2003) *Nature* 424:643–650.
9. Akeda Y, Galán JE (2005) *Nature* 473:911–915.

10. Koonin EV (1993) *Nucleic Acids Res* 21:2541–2547.
11. Claret L, Susannah CR, Higgins M, Hughes C (2003) *Mol Microbiol* 48:1349–1355.
12. Fan F, Macnab RM (1996) *J Biol Chem* 271:31981–31988.
13. Minamino T, Kazetani K, Tahara A, Suzuki H, Furukawa Y, Kihara M, Namba K (2006) *J Mol Biol* 360:510–519.
14. Vogler AP, Homma M, Irikura VM, Macnab RM (1991) *J Bacteriol* 173:3564–3572.
15. Lane MC, O'Toole PW, Moore SA (2006) *J Biol Chem* 281:508–517.
16. Miwa K, Yoshida M (1989) *Proc Natl Acad Sci USA* 86:6474–6478.
17. Minamino T, Macnab RM (2000) *Mol Microbiol* 37:1494–1503.
18. Thomas J, Stafford GP, Hughes C (2004) *Proc Natl Acad Sci USA* 101:3945–3950.
19. González-Pedrajo B, Minamino T, Kihara M, Namba K (2006) *Mol Microbiol* 60:984–998.
20. Walker JE, Saraste M, Runswick MJ, Gay NJ (1982) *EMBO J* 1:945–951.
21. Abrahams JP, Leslie AG, Lutter R, Walker JE (1994) *Nature* 370:621–628.
22. Menz RI, Walker JE, Leslie AG (2001) *Cell* 106:331–341.
23. Dreyfus G, Williams AW, Kawagishi I, Macnab RM (1993) *J Bacteriol* 175:3131–3138.
24. Futai M, Noumi T, Maeda M (1989) *Annu Rev Biochem* 58:111–136.
25. Nadanaciva S, Weber J, Wilke-Mounts S, Senior AE (1999) *Biochemistry* 38:15493–15499.
26. Pallen MJ, Bailey CM, Beatson SA (2006) *Protein Sci* 15:935–941.
27. Yoshida M, Muneyuki E, Hisabori T (2001) *Nat Rev Mol Cell Biol* 2:669–677.
28. Shirakihara Y, Leslie AGW, Abrahams JP, Walker JE, Ueda T, Sekimoto Y, Kambara M, Saika K, Kagawa Y, Yoshida M (1997) *Structure (London)* 15:825–836.
29. Patel S, Latterichi M (1998) *Trends Cell Biol* 8:65–71.
30. Lenzen CU, Steinmann D, Whiteheart SW, Weis WI (1998) *Cell* 94:525–536.
31. Yu RC, Hanson PI, Jahn R, Brünger A (1998) *Nat Struct Biol* 5:803–811.
32. Bochtler M, Hartmann C, Song HK, Bourenkov GP, Barunik HD, Huber R (2000) *Nature* 403:800–805.
33. Noji H, Yasuda T, Yoshida M, Kinosita K (1997) *Nature* 386:299–302.
34. Boyer PD (1997) *Annu Rev Biochem* 66:717–749.
35. Lupas AN, Martin J (2002) *Curr Opin Struct Biol* 12:746–753.
36. Minamino T, Imada K, Tahara A, Kihara M, Macnab RM, Namba K (2006) *Acta Crystallogr F* 62:973–975.
37. Leslie AGW (1992) *Protein Crystallogr* 26:27–33.
38. Collaborative Computational Project 4 (1994) *Acta Crystallogr D* 50:760–763.
39. Terwilliger TC, Berendzen J (1999) *Acta Crystallogr D* 55:849–861.
40. Jones TA, Zou JY, Cowan SW, Kjeldgaard M (1991) *Acta Crystallogr A* 47:110–119.
41. Brünger AT, Kuriyan J, Karplus M (1987) *Science* 235:458–460.
42. Brünger AT, Adams PD, Clore GM, DeLano WL, Gros P, Grosse-Kunstleve RW, Jiang JS, Kuszewski J, Nilges M, Pannu NS, *et al.* (1998) *Acta Crystallogr D* 54:905–921.